Comparison of K^+ and Li^+ ion scattering from Au nanoclusters deposited on SiO_x

2010 J. Phys.: Condens. Matter 22 084009

(http://iopscience.iop.org/0953-8984/22/8/084009)

J. Phys.: Condens. Matter **22** (2010) 084009 (6pp) doi:10.1088/0953-8984/22/8/084009

Comparison of K^+ and Li^+ ion scattering from Au nanoclusters deposited on SiO_x

Snjezana Balaz and Jory A Yarmoff

Department of Physics and Astronomy, University of California, Riverside, CA 92521, USA

Received 7 October 2009, in final form 11 December 2009
Published 4 February 2010
Online at stacks.iop.org/JPhysCM/22/084009

Abstract
The scattering of low energy alkali ions is used to probe the atomic and electronic structures of Au nanoclusters grown onto an untreated silicon (111) wafer. Charge-state-resolved time-of-flight spectra were collected for 2 keV $^7Li^+$ and $^{39}K^+$ as a function of Au coverage. The shapes of the spectra are interpreted in terms of the shadow cones formed by incoming Li^+ and K^+. The differences in neutralization are interpreted in terms of the ionization potentials. The results indicate that nanoclusters displaying quantum size effects are formed upon the initial Au deposition, and they evolve to multilayer nanoclusters after a critical coverage has been reached. When sufficient Au is deposited, a thick film is formed with the properties of the bulk metal.

(Some figures in this article are in colour only in the electronic version)

1. Introduction

The scattering of low energy ions is most commonly used to obtain information about the atomic structure at a surface [1]. As a low energy ion interacts with the surface, electronic transitions, such as charge exchange, promotion of the projectile to an excited state, and electron emission, also occur. These electronic transitions, which are analogous to those that take place during desorption induced by electronic transitions (DIET) processes, offer further insight into surface properties.

Professor Ted Madey was a pioneer, not only of DIET, but also of other related techniques, including low energy ion scattering and ion transmission [2–8]. Professor Madey's group used ion scattering to investigate the growth of metal films on oxide substrates, studied the transmission of very low energy ions through thin films and investigated the depth of the origin of ions produced via DIET. In addition, his group was among the first to report the formation of small Au nanoclusters deposited on TiO_2(110) [9].

Small metal nanoclusters have attracted enormous attention in the past ten years due to their inherent quantum size behavior and their potential for use in a diverse set of applications, such as catalysis [10–12]. The catalytic activity of small Au clusters is very high, despite the fact that Au metal itself is inert. Many groups have investigated the formation of Au clusters by direct deposition on oxide surfaces, such as TiO_2, SiO_2, and MgO [13–15]. In general, the growth of the Au nanoclusters is nucleated at defects, and the size of the nanoclusters increases as more Au is deposited.

In this paper, low energy alkali ion scattering is employed to probe the atomic and electronic structures of Au nanoclusters grown on SiO_x. There are certain advantages of ion scattering over other surface sensitive techniques, such as scanning tunneling microscopy (STM) or photoelectron spectroscopy. For one, ion scattering provides the ability to quickly monitor the electronic properties of clusters *in situ* while a growth parameter, such as the amount of Au deposited, is continuously varied. Unlike valence band photoelectron spectroscopy, the energy of the scattered ions can be used to completely decouple any signal arising from the substrate. In addition, ion scattering can be performed on rough surfaces that could not be easily imaged with STM.

This paper compares the scattering kinematics and the charge exchange of $^7Li^+$ to that of $^{39}K^+$. The shape of the scattered ion spectra is sensitive to the atomic structure of the nanoclusters, while the degree of charge exchange during low energy alkali ion scattering provides a measure of the quantum size behavior [16–19]. We are able to follow the growth of the clusters from single to multiple layer structures, show that the clusters display quantum size effects and demonstrate they are negatively charged while adsorbed atop the SiO_x. The shapes of the Li and K spectra are related to their shadow cone sizes, while the differences in neutralization are due to their different ionization potentials.

2. Experimental procedure

The sample preparation and subsequent measurements were carried out in an ultra-high vacuum (UHV) chamber with base

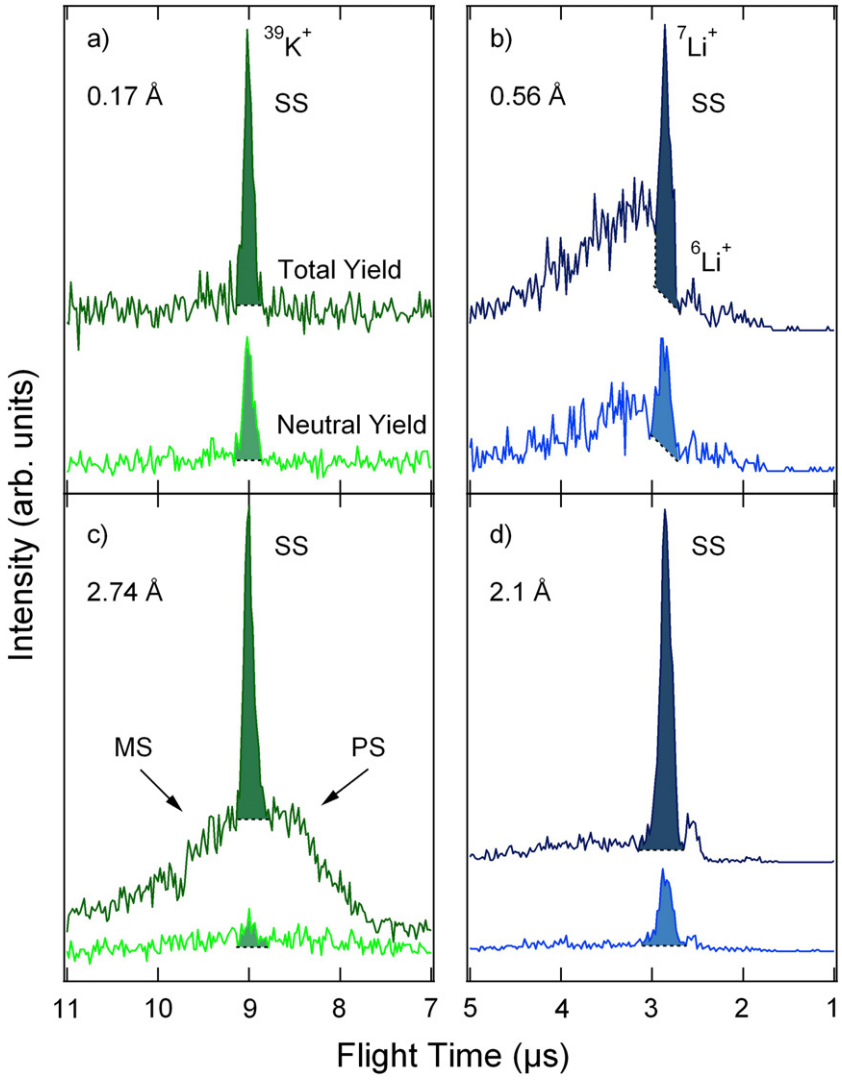

Figure 1. 'Total yield' and 'neutral yield' spectra for scattering 2 keV $^{39}K^+$ ((a) and (c)) and $^{7}Li^+$ ((b) and (d)) from Au deposited on SiO_x. The scattering angle was 135° and the spectra were collected at normal emission. Note: SS is single scattering peak, MS is multiple scattering, and PS is plural scattering.

pressure of 5×10^{-11} Torr. Prior to nanocluster growth, the untreated Si(111) substrates were annealed at 475 K for 20–30 min to desorb water and loosely bound hydrocarbons. This annealing step does not remove the native oxide layer, but instead leaves a disordered surface covered with SiO_2 and suboxides, which we denote as SiO_x [20]. Au was deposited from an evaporator that consisted of Au wire (Johnson Matthey, 99.998%) wrapped around a W filament (Mathis). Deposition occurred at a rate of ∼4 Å min^{-1}, as calibrated *in situ* with a quartz crystal microbalance. The sample cleanliness and Au deposition were monitored with Auger electron spectroscopy.

Time-of-flight (TOF) was used to collect charge-resolved spectra for scattered 2 keV $^{39}K^+$ and $^{7}Li^+$ ions [21]. The ion beam was deflected across a 1 mm^2 aperture to produce 120 ns pulses at a rate of 80 kHz. Because the beam is pulsed, the total integrated current is relatively small. This enables data to be collected while keeping the total dose to well below 1% of a monolayer, thus eliminating any significant beam damage effects. The incident beam was oriented 45° from the surface normal, while the sample normal was aimed directly towards the micro-channel plate detector. Ions and neutrals scattered at 135° were detected after traveling through a 0.635 m long flight tube containing a pair of stainless steel deflection plates. The deflection plates were grounded to collect 'total yield' spectra, while 300 V was placed between the plates to remove scattered ions and collect the 'neutral yield' spectra.

3. Results and discussion

Figure 1 shows characteristic TOF spectra for 2 keV $^{39}K^+$ (figures 1(a) and (c)) and $^{7}Li^+$ (figures 1(b) and (d)) scattered from different coverages of Au grown on SiO_x. The spectra are displayed with respect to the flight time in reverse order, as shorter times correspond to larger scattered energies. The upper spectra in each panel are 'total yield', while the lower spectra are the 'neutral yield'.

The spectra in figure 1 are each dominated by an intense peak that is due to quasi-single scattering (SS) from Au. In SS, the ion backscatters into the detector at a large angle after suffering a single binary elastic collision with a surface atom [1]. The energy loss in such a collision is a function of the relative masses of the projectile and target atom. The SS peaks at 9.0 and 2.9 μs refer to a $^{39}K^+$ or $^7Li^+$ projectile, respectively, that has scattered from a surface Au atom. The flight times differ for the two projectiles as K is heavier than Li and thus takes a longer time to reach the detector. In the case of Li (figures 1(b) and (d)), there is an additional, less intense SS peak at ∼2.6 μs, which corresponds to a lighter isotope, $^6Li^+$, scattering from Au. The abundances of $^6Li^+$ and $^7Li^+$ are 7.6% and 92.4% respectively [22], which is reflected in the relative intensities of the SS peaks. Additional features in the ion scattering spectra depend on the atomic structure of the material. For scattered K, there are additional features only at the larger Au coverages. For Li, there are additional features only at the small coverages.

The lack of additional features in the low coverage K spectra is a result of the mass differences between the projectile and the substrate. Since K is heavier than the substrate components (Si and O), projectiles that interact with the substrate can only be scattered in the forward direction. Thus, the projectiles that fail to backscatter from Au instead become embedded in the crystal. The substrate is thus essentially invisible to K^+ ion scattering.

After the Au coverage reaches about 0.5 Å, shoulders develop in the K spectra, as seen in figure 1(c). These shoulders are due to impinging ions that undergo multiple scattering (MS) and plural scattering (PS) within an Au cluster [23]. In PS, as suggested by the name, the ion experiences two or more forward, in-plane collisions, which results in a higher scattered energy than with SS [23–25]. In MS, the ion scatters from two or more atoms in a direction that is out of plane and therefore loses more energy than in an SS collision. The PS and MS trajectories require that there be a collection of Au atoms in close proximity to each other.

For small coverages of Au, Li spectra show some scattering at lower energies than the $^7Li^+$ SS peak, which is the result of MS within the substrate. Since Li is lighter than Si and O, it can make single or multiple collisions with the substrate and still backscatter. These MS features are absent after a coverage of 1.7 Å is reached, as represented in figure 1(b), since there is now Au covering much of the surface and there are consequently few open areas of exposed substrate. It is interesting to note that there are no MS or PS features when Li scatters from multiple layers of Au.

Figure 2 shows the integrated intensity of the SS peak of the 'total yield' spectra for the scattering of 2 keV $^{39}K^+$ and $^7Li^+$ as a function of Au coverage. Note that the intensities of the SS peaks in figure 2 for each alkali ion are arbitrary relative to each other. An estimated intensity area is illustrated in each panel of figure 1, and the peaks are shaded to indicate how the contribution from SS is determined by integration after background subtraction. As seen in figure 2, the intensity of the SS for both alkali ions continually increases with coverage, which is consistent with a continuous growth in the size of

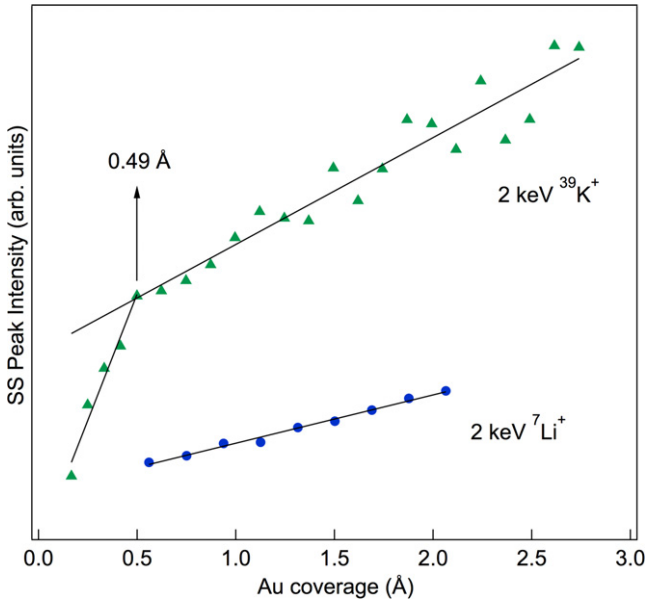

Figure 2. Intensity of the SS peak in the 'total yield' spectra for 2 keV $^{39}K^+$ and $^7Li^+$ as a function of the amount of Au deposited on SiO_x.

the Au clusters. The intensity of $^7Li^+$ has a steady linear increase with coverage over the range investigated, while the slope of the $^{39}K^+$ intensity abruptly changes at around 0.5 Å and then continues to increase linearly. This change in the slope of the $^{39}K^+$ SS peak intensity suggests the formation of multilayer structures above 0.5 Å of deposited Au, which is consistent with the change in spectral shape that occurs at this same coverage. The $^7Li^+$ SS peak intensity similarly has an uninterrupted linear increase in the range investigated, which is above 0.5 Å.

To understand the differences in the kinematical behavior of these two alkali ions, we can utilize the concept of shadowing. During the interaction between a projectile and an isolated target atom, the region into which no ion can penetrate is referred to as the shadow cone [1, 26]. Figure 3 shows the projections onto the second layer of the shadow cones formed from K and Li ions impinging on the outermost layer of an Au(111) surface. These calculations were executed in MATLAB using Oen's analytical expression [26]. The geometry corresponds to our experimental set up in which the ion beam is incident at 45° from the surface normal. The closed packed Au(111) surface was chosen for this illustration as it is the limiting case in which the Au atoms are as close to each other as can be. In reality, the actual clusters are not well ordered and therefore could have larger spacings between the atoms. The shadow cone radius formed by K ions is larger than the one formed by Li due to its larger mass.

The shadow cone size helps to explain the shape of the SS peak intensity with Au coverage for 2 keV $^{39}K^+$ scattering (figure 2). The outermost surface atoms that interact with K projectiles cast a shadow over the second layer that completely encloses them, as seen in the upper panel of figure 3. Thus, incident K ions can only see the outermost layer. When enough Au is deposited to begin the formation of a second layer, the

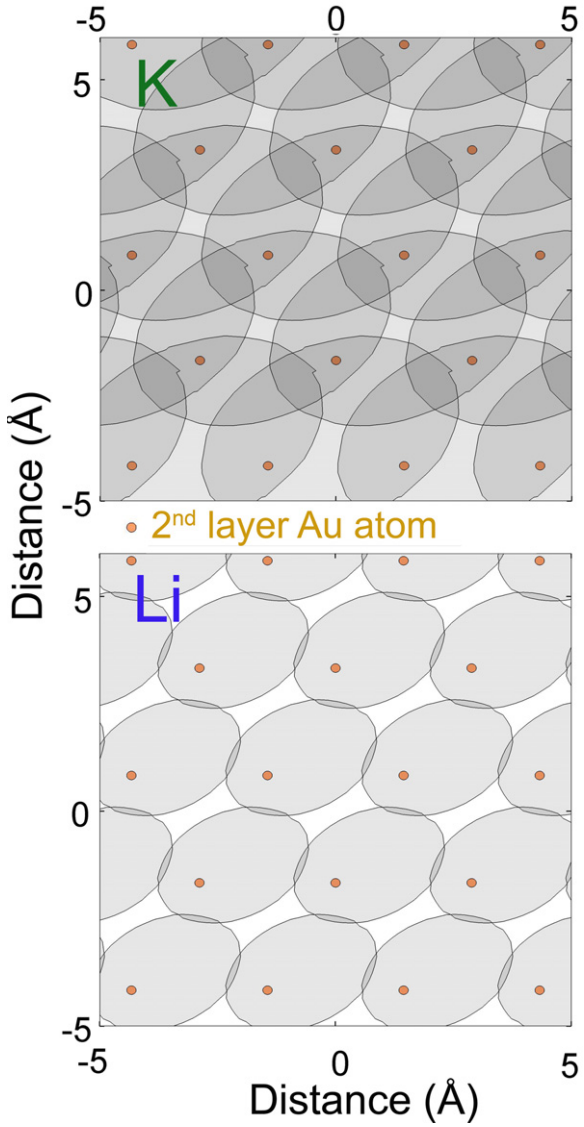

Figure 3. Shadow cones projected over the second layer of an Au(111) crystal from K and Li projectiles incident at 45° from the normal and oriented along a [11$\bar{2}$] azimuth. The small filled circles indicate the positions of the Au atoms in the second layer. The distance between the layers in Au(111) is 2.35 Å.

slope of the SS peak intensity changes since a fraction of the additional Au atoms is now shadowing those below. This change in slope occurs after 0.5 Å of Au has been deposited, confirming the formation of multilayers that was inferred from the appearance of MS and PS features in the TOF spectra.

In contrast, the shadow cones formed by 2 keV $^{7}Li^{+}$ projectiles do not completely cover the second layer, as seen in the bottom panel of figure 3. The cones, as drawn, would shadow the atoms in the second layer of a (111) surface with this incidence direction. The actual structure of the nanoclusters is disordered, however, and the (111) surface is the limit in which the Au atoms are as close to each other as possible. Thus, for the actual clusters the cones would be further spread out and there could easily be Au atoms in locations that are not shadowed. Thus, the calculation shows that under certain conditions, the Li can see more than one

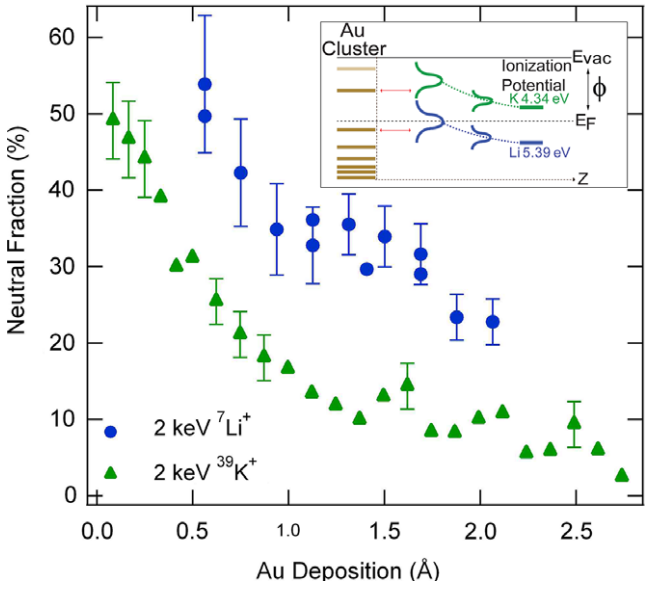

Figure 4. Neutral fractions of 2 keV $^{39}K^{+}$ and $^{7}Li^{+}$ ions scattered from Au deposited on SiO_x. Inset: schematic representation of the resonant charge transfer process for Li and K interacting with nanoclusters.

layer. How much more will depend on the details of the material and the ion beam incidence direction.

Figure 4 shows the neutral fractions of scattered 2 keV $^{39}K^{+}$ and $^{7}Li^{+}$ particles as a function of Au coverage. The neutral fraction of the scattered projectiles was determined by dividing the integrated single scattering peaks from the 'neutral yield' spectra by those of the 'total yield' spectra [21]. The first step in calculating the neutral fractions is to subtract a background from each SS peak. The shaded areas in figures 1(a)–(d) show how typical SS backgrounds were estimated and peak areas chosen. Note that there is some error involved in selecting the background since the border between SS and MS is not always well defined, and this error is considered along with statistical errors to create the error bars that are incorporated into figure 4. Note that the error bars are larger for the smaller coverages due to the lower number of scattering sites on the surface.

The changes in the neutralization of Li^{+} and K^{+} with Au coverage are qualitatively similar. As seen in figure 4, the neutral fraction of scattered $^{39}K^{+}$ particles starts at ∼50% for the smallest coverage (0.08 Å) and approaches zero with increasing deposition. The data for Li starts at a higher coverage (0.56 Å) and the neutral fractions also decrease with deposition. On average, the neutral fractions of Li are ∼20% higher than for K.

The neutralization of low energy alkali ions scattered from a metal surface is most often described as a non-adiabatic resonant charge transfer process, which depends on the ionization potential of the projectile, the local surface potential of the target and the velocity of the projectile as it exits the material [27, 28]. There are other effects that can contribute to the neutralization in specialized cases [29–31]. The general concept considers how the atomic ionization level is modified while the projectile is in the vicinity of the surface.

First, it is subject to its image charge in the metal, which causes the level to move up in energy. Second, the initially sharp ionization level broadens due to overlap with the surface states. Electrons can then transfer between the surface and the modified ionization level. This is illustrated in the inset to figure 4. Because the scattering occurs on a very short timescale, the charge transfer process is non-adiabatic and the final charge-state distribution is effectively 'frozen-in' as the projectile escapes from the surface. The point at which this occurs is a function of the projectile velocity. Typical 'freezing distances' are on the order of a few angstroms. Although this formalism was developed for metal surfaces, the general concept is still applicable to scattering from nanomaterials.

It was previously demonstrated that neutralization of low energy alkali ions scattered from nanoclusters directly probes their quantum size behavior [16–19]. The inset in figure 4 schematically illustrates how the filled states in the clusters can couple to the broadened and shifted ionization level of the projectiles. The dashed horizontal line illustrates where the Fermi level of bulk Au would be positioned, and the K and Li ionization levels are shown on the right. The Au work function ($\phi = 5.10$ eV) is larger than the K ionization (4s) level (ionization potential = 4.34 eV) and smaller than that of the Li ionization (2s) level (ionization potential = 5.39 eV), so that the Fermi energy is in between the ionization levels. The left side of the inset is a qualitative depiction of where atomic-like states could exist in a cluster. The horizontal arrows indicate how electrons can transfer between those states and the shifted and broadened ionization levels during the ion–cluster interaction. Note that the magnitude of the broadening and shifting may not be the same for an alkali projectile interacting with a cluster as with a metal surface, since both the image charge and the overlap in projectile–target states depend on the surface properties, but the general behavior is still correct.

It has been suggested that small Au clusters are partially negatively charged [32, 33], so that filled states could lie above what would be the Fermi energy in a metal. Thus, more neutrals can be produced in scattering from small Au nanoclusters than from Au metal [16–19]. As more metal is deposited, the average size of the clusters increases and the filled states move down in energy so that the degree of neutralization changes. The neutral fractions of Li, Na, and K ions scattered from these clusters generally decrease with increasing cluster size [17–19].

When sufficient Au is deposited to form a bulk-like film, there are no neutrals produced from scattered K^+ because the ionization level is well above the metal Fermi energy, as was shown in our earlier work for Au grown on TiO_2 [19]. The reason that the K neutral fraction in the present data does not go completely to zero is most likely because the amount of Au deposited in these experiments was not enough to completely form the bulk-like film. At most, we deposited about 1 monolayer (1 ML $\approx$ 2.6 Å). Also, it would take more Au to reach the thin film limit because of the rough nature of the SiO_x substrate than with a flat surface, such as $TiO_2(110)$. For scattered Li^+, the ionization level is below the metal Fermi energy, so that the neutral fraction in scattering from Au metal remains finite, as with an Au film grown on TiO_2 [17].

Since neutrals are produced when $^{39}K^+$ is scattered from the nanoclusters, as seen in figure 4, it is clear that electronic states are formed in the Au clusters during the deposition of Au onto SiO_x, and that these clusters are negatively charged. The decrease of the neutral fraction with Au deposition for both K and Li indicates changes in the quantum state occupancy with cluster size, i.e. larger Au coverages do correspond to larger cluster sizes. The difference in the K and Li ionization potentials explains the quantitative difference in neutral fractions between the two ions. Since Li has a larger ionization potential than K, it would generally be expected to produce more neutrals. Note that this behavior is not always the case when discrete states in the projectile are interacting with discrete states in a cluster [17].

The neutral fraction of K^+ scattered from Au clusters on SiO_x is more than twice that for Au clusters grown on $TiO_2(110)$, e.g. ~50% versus ~20% [19]. Two possible explanations for this are (1) smaller clusters are formed on SiO_x, or (2) there is more charge transfer to the Au clusters from the SiO_x substrate than from TiO_2. Smaller clusters could be a result of hindered surface diffusion of Au atoms across the rough SiO_x surface. More charge transfer from the untreated SiO_x sample could result from a higher defect concentration, in which electrons associated with Si dangling bonds could transfer to the clusters. More experiments are planned in order to sort out the reasons behind these substrate effects.

4. Conclusions

We investigated the differences in low energy K^+ and Li^+ scattering to better understand the physical and electronic properties of Au clusters grown on SiO_x. We used TOF to measure the charge-state-resolved kinetic energy distributions of the scattered alkali ions. The shapes of the spectra and the intensity of the SS peaks indicate the transition from single to multilayer structures. The neutral fractions of both K^+ and Li^+ ions decrease with deposition, highlighting changes in the quantum state occupancy with cluster size.

Acknowledgment

The authors wish to acknowledge R D Gann for writing the MATLAB code and providing assistance with the shadow cone projections.

References

[1] Rabalais W J 2003 *Principles and Applications of Ion Scattering Spectrometry: Surface Chemical and Structural Analysis* (New York: Wiley)
[2] Akbulut M, Sack N J and Madey T E 1997 *Surf. Sci. Rep.* **28** 177
[3] Pan J M, Diebold U, Zhang L Z and Madey T E 1993 *Surf. Sci.* **295** 411
[4] Pan J M and Madey T E 1993 *Catal. Lett.* **20** 269
[5] Pesty F, Steinruck H P and Madey T E 1995 *Surf. Sci.* **339** 83
[6] Raschke M B and Madey T E 1998 *Phys. Rev.* B **58** 15832
[7] Sack N J, Akbulut M and Madey T E 1994 *Phys. Rev. Lett.* **73** 794
[8] Sack N J, Akbulut M and Madey T E 1995 *Surf. Sci.* **334** L695

[9] Zhang L, Cosandey F, Persaud R and Madey T E 1999 *Surf. Sci.* **439** 73
[10] Haruta M 1997 *Catal. Today* **36** 153
[11] Haruta M 2004 *Gold Bull.* **37** 27
[12] Hutchings G J and Haruta M 2005 *Appl. Catal.* A **291** 2
[13] Min B K, Wallace W T and Goodman D W 2006 *Surf. Sci.* **600** L7
[14] Goodman D W 2004 *Dekker Encyclopedia of Nanoscience and Nanotechnology* ed J A Schwarz, C I Contescu and K Putyera (New York: Dekker) p 611
[15] Kitchin J R, Barteau M A and Chen J G 2003 *Surf. Sci.* **526** 323
[16] Liu G F, Sroubek Z and Yarmoff J A 2004 *Phys. Rev. Lett.* **92** 216801
[17] Liu G F, Sroubek Z, Karamakar P and Yarmoff J A 2006 *J. Chem. Phys.* **125** 054715
[18] Canario A R and Esaulov V A 2006 *J. Chem. Phys.* **124** 224710
[19] Liu G F, Karmakar P and Yarmoff J A 2007 *J. Vac. Sci. Technol.* A **25** 1133
[20] Grunthaner F J and Grunthaner P J 1986 *Mater. Sci. Rep.* **1** 65
[21] Weare C B and Yarmoff J A 1996 *Surf. Sci.* **348** 359
[22] Lide D R 1992 *Handbook of Chemistry and Physics* (Boca Raton, FL: CRC Press)
[23] Draxler M, Beikler R, Taglauer E, Schmid K, Gruber R, Ermolov S N and Bauer P 2003 *Phys. Rev.* A **68** 1
[24] Brongersma H H, Draxler M, de Ridder M and Bauer P 2007 *Surf. Sci. Rep.* **62** 63
[25] Keller C A, DiRubio C A, Kimmel G A and Cooper B H 1994 *Phys. Rev. Lett.* **75** 1654
[26] Oen O S 1983 *Surf. Sci.* **131** L407
[27] Los J and Geerlings J J C 1990 *Phys. Rep.* **190** 133
[28] Behringer E R, Andersson D R, Cooper B H and Marston J B 1996 *Phys. Rev.* B **54** 14765
[29] Behringer E R, Andersson D R, Cooper B H and Marston J B 1996 *Phys. Rev.* B **54** 14780
[30] Canario A R, Kravchuk T and Esaulov V A 2006 *New J. Phys.* **8** 7
[31] Niedfeldt K, Nordlander P and Carter E A 2006 *Phys. Rev.* B **74** 5
[32] Sanchez A, Abbet S, Heiz U, Schneider W D, Häkkinen H, Barnett R N and Landman U 1999 *J. Phys. Chem.* **103** 9573
[33] Chrétien S and Metiu H 2007 *J. Chem. Phys.* **126** 104701